ROBUST TEXTURE CLASSIFICATION USING WAVELET FRAMES

MAUSUMI ACHARYYA(*) AND MALAY K. KUNDU(*)

Machine Intelligence Unit
Indian Statistical Institute
203. B. T. Road. Calcutta - 700 035, INDIA
(*) e-mail :{res9522, malay}@isical.ac.in

Abstract. In this paper we present an approach to characterize textures at multiple scales using wavelet transforms and discuss the issues of translational and rotational invariance and noise immunity of a texture analysis system. We employ the non-separable discrete wavelet frames analysis which gives an overcomplete wavelet decomposition. Discrete Wavelet Frame (DWF) decompose the textures into a set of frequency channels. A texture is characterized by a set of these channel variances in this work. Classification experiments using twenty Brodazt textures indicate that texture signatures based on wavelet frame analysis are beneficial for accomplishing subtle discrimination of textures and robust classification against rotation translation and noise.

Key words. Feature extraction, texture classification, wavelet transform, wavelet frames, non-separable filters.

1 Introduction

Effective classification and segmentation of images based on textural features is of key importance in applications like image analysis, remote sensing, robot vision, query by content in large image data bases and many others. A wide variety of texture analysis methods have been proposed in the past [1] [2]. Earlier approaches focused on first-order and second-order statistics of textures [3] [4], description using texture primitives and system rules [5]. There has been an extensive study on model based approaches like Markov random fields [6] [7] and local linear transforms [8]. All these approaches are restricted to the analysis of spatial interactions over relatively small neighborhoods, and are best suited for analysis of micro textures.

Psychovisual studies reveals that the human visual system processes images by decomposing them into filtered images of various frequencies and orientation at different scales that is capable of preserving both local and global information. This multiscale processing of the human visual system is a strong motivation for texture analysis methods based on these concepts [9] - [12] . An extensive study has been made which certainly reveals the superiority of these multiscale processing over the more traditional ones mentioned above.

Multiresolution techniques intend to transform

images into representation in which both frequency and spatial information is present. Wavelet theory provides a more formal, precise and unified approach to multiresolution representations [13] [14]. The importance of scale in texture descriptions is clear from the change in appearance of most textures when viewed in different resolutions, and from the empirical division into micro and macro textures. These recent findings have motivated several important studies for texture analysis [15], [16], [17], [18], [19], [20] .

The majority of the existing work on texture analysis assumes that the viewing angle of all images are the same. Practically this is an unrealistic assumption. A texture analysis approach should ideally be invariant to orientation of the texture. The standard dyadic wavelet transform performs a frequency splitting in octave bands, which suffice for many texture analysis problems but may be too coarse for detailed texture analysis. The work by Chang and Kuo [21], however, indicate that texture features are most prevalent in intermediate frequency bands. This proposal has been studied with a particular attention to the use of wavelet packets [22]. But its performance deteriorates when rotation of textured images is considered.

Kashyap *et.al* [7] first recognized the importance of rotation-ivariant texture feature extraction. He developed a texture classification scheme based on autoregresive (AR) model. But this model peroformed poorly for textures with strong anistropy. Cohen *et.al* [23] modeled textures as Gaussian random fields and used maximum likelihood (ML) method to estimate the coefficients and rotation angles. But this algorithm is computationally expensive. Chen and Kundu [24] used multichannel subband decomposition and a hidden Markov model (HMM) and incorporation of rotated samples in the training data to solve this problem. Other works on rotational invariance involves spiral resampling of the data, to obtain a 1-dimensional signal, where rotation invariance is simulated as translation invariance [25]. Most recently Fountain *et. al* [26] have worked on rotation invariant texture classification by taking the Fourier trandform (FT) of the gradient direction histograms of the textures. The direction histograms being a periodic function of 2π, a rotation is reflected as a translation in the fourier domain. Therefore the fourier coefficients give the rotational invariant features.

In this paper, texture properties are characterized by wavelet frame analysis. While discrete wavelet transform gives a non redundant representation of the textures. the discrete wavelet frame uses an overcomplete representation. This technique is employed to study the performance of a texture classifier with respect to rotational and translational invariance and immunity to noise.

In many texture analysis problems, rotational information is needed. We conjecture that if the rotational information is used directly to generate the texture features we can achieve the desired classification very efficiently.

Due to the separable nature of implementation of the two dimensional discrete wavelet transform, it is strongly oriented in the horizontal and vertical directions. Such a decomposition cannot efficiently characterize directions other than 0^0 and 90^0. Therfore the solution is to take resort to a non-separable nature of implementation of the wavelet transform in 2-D.

Another important drawback of the DWT is that, a simple integer shift of the input signal will yield a completely different wavelet transform. A feature extraction scheme has to be independent of any translational shift, for texture has translation invariance (or stationary) property. A solution to overcome this limitation is to compute the discrete wavelet transform for all pos-

sible integer shifts of the input signal [20]. This approach leads to the redundant DWF in which the wavelet decomposition is carried out without downsampling. This entails that a better characterization of the texture statistics is possible.

Moreover the orthogonal or non redundant DWT requires that the transfer functions of the decomposing filters do not overlap each other and are confined within rectangular regions in the frequency domain. With this type of localization of the transfer functions it is very difficult to extract rotation and translation invariant features. What we need is smooth transfer functions of the decomposing filters, and appreciable overlapping of these in the frequency domain. This leads to the redundant wavelet frames which uses non-orthogonal basis set.

Another crucial point is that a multiresolution decomposition of the textures inherently performs regularization against noise. This suggests that such analysis can provide a powerful method for accomplishing robust texture classification. compared to traditional single resolution techniques.

In the next section, we review the wavelet frame decomposition. Section 3 describes the wavelet parameter computation which gives the features for texture discrimination. Section 4 presents our strategy and experimental design. In section 5 we present our results and critical remarks about the performance with respect to the several parameters considered in our investigation and finally, summarize the results and conclude our study.

2 Wavelet transforms and wavelet frames

2.1 Discrete wavelet transform

The wavelet decomposition can be interpreted as signal decomposition in a set of independent, spatially oriented frequency channels. Under these constraints an efficient real space implementation of the transform using quadrature mirror filter exists [14]. The discrete normalized scaling and wavelet basis functions are defined as,

$$\begin{aligned} \phi_{i,k}(l) &= 2^{i/2} h_i(2^i l - k) \\ \psi_{i,k}(l) &= 2^{i/2} g_i(2^i l - k) \end{aligned} \tag{1}$$

where i and k are the dilation and translation parameters and h_i and g_i are respectively the sequence of lowpass and bandpass filters of increasing width indexed by i, which are expanded by inserting an appropriate number of zeros between taps and satisfy the quadrature mirror filter condition. The full discrete wavelet expansion of a signal $x \in l_2$ (l_2 is the space of square summable functions)

$$x(l) = \sum_{k \in Z} c_{(d_0)}(k)\phi_{d_0,k} + \sum_{i=1}^{d_0} \sum_{k \in Z} d_{(i)}(k)\psi_{i,k} \tag{2}$$

$d_{(i)}$'s are the wavelet coefficients and $c_{(d_0)}$'s are the expansion coefficients of the coarser signal approximation $x_{(d_0)}$. The c_{d_0}'s and d_i's can be interpreted in terms of simple filtering and downsampling operations.

$$\begin{cases} c_{(d_0)}(k) &= 2^{d_0/2}[h_{d_0}^T * x]_{\downarrow 2^{d_0}(k)} \\ d_{(i)}(k) &= 2^{i/2}[g_i^T * x]_{\downarrow 2^i(k)} \\ & \qquad \text{for} \quad i = 1, \cdots, d_0 \end{cases} \tag{3}$$

where the symbol ^{T} denotes the transpose operation ($i.e. h^T(k) = h(-k)$) and where $[.] \downarrow m$ is the downsampling by factor m. In practice the 2-D DWT is computed by applying a separable filter bank to the image.

$$c_i(x,y) = [h_{i,x} * [h_{i,y} * c_{i-1}]_{\downarrow 2,1}]_{\downarrow 1,2}(x,y) \tag{4}$$

$$d_i^1(x,y) = [h_{i,x} * [g_{i,y} * c_{i-1}]_{\downarrow 2,1}]_{\downarrow 1,2}(x,y) \tag{5}$$

$$d_i^2(x,y) = [g_{i,x} * [h_{i,y} * c_{i-1}]_{\downarrow 2,1}]_{\downarrow 1,2}(x,y) \tag{6}$$

$$d_i^3(x,y) = [g_{i,x} * [g_{i,y} * c_{i-1}]_{\downarrow 2,1}]_{\downarrow 1,2}(x,y) \tag{7}$$

$*$ denotes the convolution operator, $\downarrow 2,1$ ($\downarrow 1,2$) denote subsampling along the rows (columns)

and $c_0 = I(x,y)$ the original 2-D signal. $h_{i,x}$ ($g_{i.x}$) and $h_{i,y}$ ($g_{i,y}$) are the lowpass (bandpass) filtering along x and y directions respectively corresponding to different scale. $c_i(x,y)$ corresponds to the lowest frequencies, the d_i^n are obtained by bandpass filtering in a specific direction and thus contain the detail information at scale i. $d_i^1(x,y)$ corresponds to the vertical high frequencies (horizontal edges), $d_i^2(x,y)$ the horizontal high frequencies (vertical edges) and $d_i^3(x.y)$ the high frequencies in both direction (the corners). $I(x,y)$ is represented at several scales by, $\{c_{d_0}, d_i^n \mid n = 1,2,3, i = 1,\ldots,d_0\}$

We can extend our discussion in defining wavelet packets as a generalization of orthonormal and compactly supported wavelets [27]. From the subband filtering point of view, the difference between wavelet packet transform (DWPT) and standard wavelet transform (DWT) is that the former recursively decomposes the high frequency components as well, unlike the other, thus resulting in a tree structured multiband extension of the wavelet transform.

2.2 Wavelet Frames

Wavelet frame leads to an overcomplete decomposition of the signal

$$\begin{cases} d_i^{DWF}(k) &= \langle g_i(l-k).x(l)\rangle_{l_2} \\ c_{d_0}^{DWF}(k) &= \langle h_d(l-k).x(l)\rangle_{l_2} \end{cases} \quad (8)$$

Due to the special structure of the analysis filter bank, this decomposition has an interesting property of energy conservation. The frame is a spanning set, that requires finite limits on an inequality bound of inner products. If we want the coefficient in an expansion of a signal to represent the signal well, these coefficients should have certain properties, that are stated best in terms of energy and energy bounds [13].

The family of sequences
$F = \{g_1(l-k), \ldots\ldots, g_{d_0}(l-k), h_{d_0}(l-k)\}$ constitutes a frame of the Hilbert space l_2, if there exists two constants $A > 0$ and $B < \infty$ such that,

$$A \cdot \|x\|_{l_2}^2 \leq \sum_{k \in Z} \langle x(l), h_d(l-k)\rangle^2 + \sum_{i=1}^{d_0} \sum_{k \in Z} \langle x(l), g_i(l-k)\rangle^2 \leq B \cdot \|x\|_{l_2}^2 \quad (9)$$

With the help of Parseval's theorem it is easy to show that the energy conservation property is preserved

$$\|x\|_{l_2}^2 = \|c_{d_0}\|_{l_2}^2 + \sum_{i=1}^{d_0} \|d_i\|_{l_2}^2 \quad (10)$$

By definition, $c_i(k) = \langle x(l), h_i(l-k)\rangle$ and $d_i(k) = \langle x(l), g_i(l-k)\rangle$. where $\langle .,. \rangle$ is the corresponding inner product. The fundamental difference with an orthogonal system is that the representation may be redundant, this property together with the definition of wavelet coefficients in (3), leads to the simple reconstruction formula

$$x(l) = \sum_{k \in Z} c_{d_0}(k) h_{d_0}(l-k) + \sum_{i=1}^{d_0} \sum_{k \in Z} d_i(k) g_i(l-k) \quad (11)$$

3 Proposed Method for feature extraction

We discuss in this section the choice of the filter bank, and the computation of the wavelet parameters used as texture features.

What we need is a nonorthogonal basis set or frames. This facilitates the decomposition of a signal in 2-dimensional space by applying one dimensional non separable filters along rows and columns independently.

The wavelet function is defined by
$\psi_a(\vec{b}) = \frac{1}{\sqrt{a}} \psi(\frac{\vec{x}-\vec{b}}{a})$.

The directional information, can be incorporated in the wavelet function, by including a rotational parameter in it [13].

$$\psi_{a.\theta}(\vec{b}) = \frac{1}{a}\psi(R^{\theta}(\frac{\vec{x}-\vec{b}}{a})) \tag{12}$$

where R^{θ} is the rotation operator denoted by the matrix

$$\begin{pmatrix} \cos\theta & -\sin\theta \\ \sin\theta & \cos\theta \end{pmatrix}$$

Now if the wavelet is circularly symmetric *i.e* R^{θ} has no influence in (12), such an wavelet would generate rotation invariant features. Therefore the wavelet function has to satisfy two conditions one is $\hat{\psi}(0) = 0$, which implies that the wavelet function has to be a zero mean function and $\hat{\psi}(\vec{r},\theta) = \hat{\psi}(\vec{r},0)$, this ensures that the rotation operator has no effect in (12), where $\hat{}$ means the Fourier domian representation. We have chosen the wavelet used by Mallat in [28], which is the second derivative of a smoothing function. This choice have been made due to the following reasons. Firstly, this closely approximates the second derivative of Gaussian, which has circular symmetry. Secondly, the basis functions are symmetrical, which means that there is no phase distortion, and that the spatial localization of the wavelet coefficients is well preserved, moreover these filters are also useful in alleviating boundary effects by simple methods of, mirror extension. The filter corresponding to the second derivative of a smoothing function can be written as $F(\omega) = \omega^2 L(\omega)$, where $L(\omega)$ is the frequency response of the smoothing low pass filter and should have a non zero value at $\omega = 0$. For the filter used $F(\omega)$ has an order 2 zero at $\omega = 0$. and exhibits sharper outband attenuation and thus better frequency separation.

3.1 Multiscale wavelet representation

The transform employed in this work is based on non-orthogonal (redundant) discrete wavelet frames introduced by Mallat [29]. Let $\phi(x,y)$ be a smoothing function. We call the smoothing function the impulse response of a lowpass filter with a total mass of one and compact support, i.e.

$$\int_{-\infty}^{\infty}\int_{-\infty}^{\infty}\phi_s(x,y)dxdy = 1$$

$$\exists\epsilon > 0 : \phi_s(x,y) = 0, \forall \mid x \mid, \mid y \mid > \epsilon. \tag{13}$$

Supposing $\phi(x,y)$ is differentiable, we define two wavelet functions, $\psi^1(x,y)$ and $\psi^2(x,y)$ such that.

$$\psi^1(x,y) = \frac{\partial^2\phi(x,y)}{\partial^2 x}$$

$$\psi^2 = \frac{\partial^2\phi(x,y)}{\partial^2 y} \tag{14}$$

Let.

$$\psi_s^1(x,y) = \frac{1}{s^3}\psi^1(\frac{x}{s},\frac{y}{s})$$

$$\psi_s^2(x,y) = \frac{1}{s^3}\psi^2(\frac{x}{s},\frac{y}{s}) \tag{15}$$

be the dilations of the functions ψ^i by a factor s and $\phi_s(x,y) = \frac{1}{s}\phi(\frac{x}{s})$ the dilation of $\phi(x,y)$ by s.

Let $I(x,y)$ be an image in 2-D and $I(x,y) \in L^2(R)$. The wavelet transform of $I(x,y)$ at scale s has two components defined by,

$$\begin{aligned} w_s^1(x,y) &= I * \psi_s^1(x,y) \\ w_s^2(x,y) &= I * \psi_s^2(x,y) \end{aligned} \tag{16}$$

s is the scale parameter which commonly is set equal to 2^i with $i = 1,\cdots,d_0$. This yields the traditional octave band wavelet transform of depth 2^{d_0}. w_s^1 and w_s^2 are referred to as the detail images, since they contain the horizontal and vertical frequency informations of I at scale s.

This transform is computed by iterative filtering by a set of lowpass filters h_i associated with the smoothing function ϕ and bandpass filters g_i associated with the wavelets ψ^1 and ψ^2. These

filters have finite impulse responses, which makes the transform fast and easy to implement.

$$\begin{aligned} c_{2^{i+1}}(x,y) &= [h_{i,x} * [h_{i,y} * c_{2^i}]](x,y) \\ w^1_{2^{i+1}}(x,y) &= [\delta_{i,x} * [g_{i,y} * c_{2^i}]](x,y) \\ w^2_{2^{i+1}}(x,y) &= [g_{i,x} * [\delta_{i,y} * c_{2^i}]](x,y) \end{aligned} \quad (17)$$

$c_1 I$ is the original image and δ is the Dirac filter whose impulse response equals 1 at 0 and 0 otherwise. $*$ denotes the convolution operator. $A * (B * C)$ denotes separate convolution of the rows and columns respectively of the image A with 1-D filters B and C.

Then the wavelet representation of depth d_0 of the image $I(x,y)$ consists of the low resolution images $\{c_{2^i}\}$ and detail images $\{w^j_{2^i}\}$ for $\{j = 1,2\}$ and $\{i = 1,\cdots,d_0\}$.

3.2 Texture features computation

Feature extraction is a crucial step in accomplishing reliable classification. A good feature representation should be consistent among the pixels with the same class, while as disparate as possible between classes for authentic and reliable classification. This means that it should reflect some global view while keeping some discrimination capability at the pixel level. Therefore the problem in general is one of spatial- spatial frequency analysis. We now discuss the computation of the rotation and translation invariant parameters from wavelet transformed images.

Substitution of (14) and (16) in (15) yields the following,

$$\begin{pmatrix} w^1_s(x,y) \\ w^2_s(x,y) \end{pmatrix} = s^2 \begin{pmatrix} \frac{\partial^2}{\partial^2 x}(I * \phi_s)(x,y) \\ \frac{\partial^2}{\partial^2 y}(I * \phi_s)(x,y) \end{pmatrix}$$

$$= s^2 \nabla^2 (I * \phi_s)(x,y) \quad (18)$$

where ∇^2 denotes the Laplacian. It defines edge magnitudes of the image and since it has the same property in all directions is invariant to rotations in the image. That is the wavelet transform of an image consists of the components which give a measure of the edge magnitudes of the image, smoothed by the dilated smoothing function ϕ_s. The edge magnitudes of the image is given as,

$$w^r_s(x,y) = \sqrt{(w^1_s(x,y))^2 + (w^2_s(x,y))^2} \quad (19)$$

The $w^r_s(x,y)$ contain a measure of the edge magnitude at (x,y), which is proportional to the magnitude of the local gray level variation of the image and clearly yields a rotation invariant multiscale representation $\{(w^r_s)_{(s=1,\cdots,2^{d_0})}, c_{d_0}\}$.

The nonsampled DWF representation gives translation invariance and since the wavelet transforms of the image are obtained form the smoothed images at successive scales the noise is inherently smoothed out in this operation of multiscale processing.

The energies of the detailed images decomposed into different frequency channels at different resolutions are given by

$$Ed_i = \frac{1}{M\ N} \sum_{x,y} (w^r_{2^i}(x,y))^2, \quad i = 1,\cdots,d_0 \quad (20)$$

Energies of the low resolution images are

$$Es_i = \frac{1}{M\ N} \sum_{x,y} (c_{2^i})(x,y))^2, \quad i = 1,\cdots,d_0 \quad (21)$$

M and N are the number of rows and columns of the digitized image $I(x,y)$.
In this approach we arrange the output of the filterbank into d_0 component subbands

$$\mathbf{f}(x,y) = (f_{2^i}(x,y))_{i=1,\cdots,d_0} =$$

$$[c_1(x,y),\ldots,c_{d_0}(x,y),\ d_1(x,y),\ldots,d_{d_0}(x,y)]^T \quad (22)$$

A more compact representation in terms of the channel variances $\mathrm{Var}\{f_{2^i}\}$ is envisaged. In practice the channel variances are estimated from the average sum of squares over a region

Reg (MXN) of the given texture. Each channel extracts a particular aspect of the texture at different frequencies and resolutions.

$$feat_{var_{2^i}} = \frac{1}{Reg} \sum_{(x,y)\ \in\ Reg} \left(f_{2^i}(x,y) - \overline{f_{2^i}}(x,y)\right)^2 \tag{23}$$

where *Reg* denotes the number of pixels in its region and $\overline{f}_{2^i}(x,y)$ is the mean value of energy of each channel. We have taken the logarithmic of these channel variances as the features.

3.2.1 Experimental validity of the assumption

Figure 3 shows some of the textured images taken from the dataset of our experiment given in Fig. 2, that we have used to generate the composite textures used in our experiment. We calculate the histograms of the edge magnitude values given by (19) of these textures at different rotations. The histograms so obtained have many local minima and maxima which can be removed by local smoothing of the histograms. This is accomplished by local averaging of neighboring histogram elements. We have taken three adjacent elements at a time and the process is repeated for a number of iterations. A plot of these histograms after smoothing is given in Fig. 4 to give a feeling that the edge magnitudes of the textures are indeed rotation invariant. We calculate the mean and second and third order central moments of the histograms corresponding to the unrotated texture and its several rotated versions, to measure the similarity between these histograms, which is given in Table 1. The percent deviation of the moments corresponding to the rotated histograms from that of the unrotated one are also tabulated. The maximum deviation happens to be only five percent. This suggests that our texture features are indeed rotation invariant.

3.3 Discrimination using K_NN classifier

Texture classification is a process whereby texture samples are assigned to a finite set of texture classes. We have resorted to a feature-based supervised classification method and have used a non-parametric classifier (K_NN) in our experiment. The representative feature vectors for each texture sample consisting of n feature elements are assigned a class labelling in the training data set, these are the exempler vectors. Classification of the unknown texture's feature vector from the test data set assigns the class of that exemplar vector to it for which the Eucleadian distance between these two vectors is minimum.

More complex classification schemes such as the neural network could be considered, but these typically depend on initialization and learning length, while K_NN classifier do not. Since we emphasize on the feature extraction scheme we take resort to this simple classifier. K_NN provides a robust and efficient classification scheme for evaluation of recognizing features and comparisons of feature sets. Also since this rule is derived from the Bayes rule, it is optimal in the sense that it minimizes the conditional risk.

3.4 Experimental data set

We performed classification experiments using 20 Brodazt textures [30] some of which are shown in Fig. 2. The original photographs were digitized and converted into 128 X 128 image arrays.

So far in texture classification problems people have usually divided each images into overlapping (or non overlapping) subregions and evaluated the feature vectors for each subregion in each class. This was adopted to increase the number of data sets. But here in this paper we have adopted a different method for extracting experimental data sets. Each class were subjected to five different translations in all direc-

tions (left, right, up and down), and oriented by five different rotations. Five different levels of Gaussian noise were incorporated in each class. There were 35 different samples of size 128 X 128 for each class which were all different from each other either in translation or noise level or rotation.The wavelet frame decomposition according to (17) was performed by processing individual images without downsampling. Each image were subjected to three levels (scale) of decomposition, and each level was represented by 6 features as shown in Fig. 1. The energies and channel variances for all the 6 subbands were computed. We chose the log of energy and variance as the information measures. The energy measure characterizes the luminance of the texture, while variance measure gives an idea about the contrast of it.

4 Results and critical comments

In the first series of experiments we compared the performance of the discrete wavelet frame (DWF) and discrete wavelet packet transform (DWPT) approaches. The basis functions of the spline wavelet that we chose for the DWF analysis are symmetrical which means that there is no phase distortion and spatial localization of the wavelet coefficients is well preserved. The DWPT (discrete wavelet packet transform) was achieved by Daubechies analyzing filter of length 16.

The data sets were evaluated using the five set of parameters shown in Table 2. The percent of correct classification was measured by the $leave - k - out\ method$. That is out of N data sets each time k distinct samples were taken as test data without repetition and the rest were used for training. We get an excellent classification result while considering the redundant DWF decomposition which is consistent with our expectation. We get very poor classification with DWPT, which supports our argument that the orthogonal transforms using separable filters are very unsuitable for feature extraction of rotated textures. We however found wavelet packet decomposition to perform quite well as a feature extractor for unrotated textures. The observation from Table 2 is that, a 45^0 rotation affects classification results. This is because some of the textures that we have used are highly anisotropic and this anisotropy is more pronounced in the diagonal direction. In the next set of experiments we changed the parameter values. We incorporated noise as high as 50 db., corrupting 70 percent of the pixels and translation as large as 64 units. This result is given in Table 3. We found that when rotation was not considered classification results were almost perfect. Errors are introduced in the images due to translation. The local periodicity of the texture elements can break due to translation by circular shift of the images. False energy peaks can emerge at the boundaries. Also incorporation of noise give rise to false energy peaks. A texture is characterized by extracting its local frequency contents. The basic idea is that some of the textures may have low energies and others may have high energies. Textures are classified with a measure of these energies. We measure the energy/ variance of the transformed images over the entire image discarding any local windowing operation for feature extraction. A local distortion is suppressed due to averaging over the entire image. The textured images are decomposed into several levels of resolution. This is accomplished by smoothing the textures and then extracting edge informations from them. The smoothing operation inherently removes most of the noise present as we go to coarser resolutions. Classification error occurs for a translation of 64 and noise level of 50 db. but is not remarkably high. This is because with such a high level of noise contamination some of the textures become almost visually indiscriminable. The rotated, translated and noisy samples of some of the textures are shown Fig. 3, Fig. 5 and Fig 6.

Table 1: Moments of the magnitude histograms tabulated for comparing the similarity between the unrotated texture histograms and their rotated versions.

Texture data	Rotation in deg	Order of moments			% deviation of moments w.r.t unrotated image		
		mean	Second	Third	mean	Second	Third
Texture 1	unrotated	1.1268	0.001449	0.001637	-	-	
	20	1.1270	0.001448	0.001636	0.02	0.06	0.06
	45	1.1286	0.001453	0.001643	0.16	0.27	0.36
	55	1.1299	0.001458	0.001651	0.28	0.62	0.85
	90	1.1264	0.001449	0.001635	0.03	0.00	0.12
Texture 2	unrotated	1.2882	0.002293	0.002961	-	-	-
	20	1.3077	0.002360	0.003073	1.51	2.92	3.78
	45	1.3134	0.002383	0.003118	1.95	3.92	5.30
	55	1.3179	0.002400	0.003121	2.30	4.45	5.40
	90	1.2919	0.002306	0.003087	0.29	2.28	4.25
Texture 3	unrotated	1.4118	0.002927	0.004145	-	-	-
	20	1.4341	0.002831	0.003935	1.57	3.27	5.06
	45	1.4190	0.002952	0.004209	0.51	0.85	1.54
	55	1.4227	0.003015	0.004332	0.77	3.00	4.51
	90	1.4055	0.002901	0.004089	0.45	0.88	1.35
Texture 4	unrotated	1.3345	0.002457	0.003288	-	-	-
	20	1.3394	0.002475	0.003324	0.36	0.73	1.09
	45	1.3361	0.002460	0.003295	0.11	0.12	0.21
	55	1.3412	0.002482	0.003337	0.50	1.01	1.49
	90	1.3311	0.002444	0.003262	0.25	0.52	0.79

We performed another experiment in which we used features for 0^0 rotation to design a classifier and tested its performance in classifying features from rotated samples ranging from 20^0 to 90^0. The results given in Table 4 clearly gives us an idea as how the classifier responds to the rotated samples of the textures. We also wanted to compare the performance of the classifier considering both the information measures used in our experiment. We found the Log of channel variance to outperform the Log energy measure. We also found from Table 5 that if we have instances of all rotations in the training data and we employ $leave - k - out\ method$ for classification of rotated data we can get excellent results. The 45^0 rotation classification is comparatively poor than the others.

So we can summarize our results as, for classification of rotated textures, multiresolution representation of the images is clearly preferable. Although texture features are prevalent in the intermediate frequency bands, which suggests that wavelet packet signatures can classify textures very efficiently, they perform very poorly when rotation is taken into account. So an overcomplete wavelet decomposition, which leads to wavelet frames happens to be a preferred solution. We also find that number of features used

Table 2: Classification performance considering the discrete wavelet frame transform and the discrete wavelet packet transform.

Test data set			Training data set			% of classifn. for	
transl.	rotn.	noise	transl.	rotn.	noise	DWF	DWPT
8	5	15	16 8 16 8	20 30 60 45	25 15 25 15	99.99	88.88
16	20	25	8 8 16 8	5 30 60 45	15 15 25 15	99.92	73.70
8	30	15	16 16 8	20 60 45	25 25 15	99.99	83.70
16	60	25	8 8 16 8	5 30 20 45	15 15 25 15	99.99	77.00
8	45	15	8 8 16 16	5 30 60 20	15 15 25 25	95.92	77.00

Table 3: Classification performance without considering rotation.

Type of decomp	No. of features	Test data set			Training data set			% of classifn.
		transl.	rotn.	noise	transl.	rotn.	noise	
DWF	6	8	0	15	16 32 64 48	0 0 0 0	25 30 50 15	99.99
		16	0	25	8 32 64 48	0 0 0 0	15 30 50 15	99.99
		32	0	30	8 16 64 48	0 0 0 0	15 25 50 15	99.99
		64	0	50	8 32 16 48	0 0 0 0	15 30 25 15	98.89
		48	0	15	8 32 64 16	0 0 0 0	10 30 50 25	99.99

Table 4: Percent of correct classification considering rotation only and comparison of the performance of the two information measures.

Training data set rotation in deg.	Test data set rotation in deg.	Information measure	Percent classifn.
0	20	Log energy	97.38
0	30		93.33
0	45		85.00
0	60		88.00
0	75		93.38
0	90		93.33
0	20	Log variance	98.82
0	30		98.82
0	45		95.29
0	60		97.64
0	75		97.64
0	90		97.64

Table 5: Percent of correct classification considering rotation only by *leave − k − out method*.

Test data set rotation in deg.	Training data set rotation in deg.	Percent classifn.
0	20 30 45 60	98.89
20	0 30 45 60	100
30	0 20 45 60	100
45	0 20 30 60	100
60	0 20 30 45	100

is only six which is really very small compared to the number of features used for classification purpose found in the literature. That is in essence we have achieved a huge reduction in dimensionality of the feature space.

In the set of textures classes that we had selected there were some textures which showed high anisotropy. For this whole series of experiments classification error usually occurred between texture pairs that were almost difficult to discriminate visually and also from textures which were highly anisotropic.

We can conclude that texture signatures based on multiresolution wavelet frames analysis holds great potential for accomplishing subtle discrimination and robust classification against rotation, translation and noise and is computationally simple and efficient.

5 References

[1] T. R. Reed and J. M. H. du Buf, "A review of recent texture segmentation and feature extraction techniques," *CVGIP: Image Understanding*, vol. 57, no. 3, pp. 359–372, 1993.

[2] M. Tuceryan and A. K. Jain, "Texture analysis," in *Handbook of Pattern Recognition and Computer vision*, pp. 235–276, World Scientific, 1993.

[3] R. M. Haralick, K. Shanmugan, and I. Dinstein, "Texture feature for image classification," *IEEE Trans. System., Man., Cybern.*, vol. 8, no. 6, pp. 610–621, 1973.

[4] P. C. Chen and T. Pavlidis, "Segemntation by texture using correlation," *IEEE Trans. Pattern Anal. Machine Intell.*, vol. PAMI-5, pp. 64–69, Jan 1983.

[5] R. M. Haralick, "Statistical and structural approaches to texture," *Proc. IEEE*, vol. 67, pp. 768–804, 1979.

[6] G. C. Cross and A. K. Jain, "Markov random field texture models," *IEEE Trans. Patt. Anal. Mach. Intell.*, vol. 5, pp. 25–39, 1983.

[7] R. L. Kashyap and A. Khotanzed, "A model-based method for rotation invariant texture classification," *IEEE Trans. Pattern Anal. Machine Intell. PAMI*, vol. 8, no. 4, pp. 472–481, 1986.

[8] K. L. Laws, "Rapid texture identification," in *Proc. SPIE*, vol. 238, pp. 376–380, 1980.

[9] A. K. Jain and F. Farrokhnia, "Unsupervised texture segmentation using gabor filters," *Pattern Recognition*, vol. 24, no. 12, pp. 1167–1186, 1991.

[10] C. C. Chen and D. C. Chen, "Multiresolution gabor filters in texture analysis," *Pattern Recognition Letters*, vol. 17, no. 10, pp. 1069–1076, 1996.

[11] A. C. Bovik, M. Clark, and W. S. Geisler, "Multichannel texture analysis using loacalized spatial filters," *IEEE Trans. Patt. Anal. Mach. Intell.*, vol. 12, pp. 55–73, 1990.

[12] M. R. Turner, "Texture discrimination by gabor function," *Biol. Cybern.*, vol. 55, pp. 71–82, 1986.

[13] I. Daubechies, *Ten Lectures on Wavelets*. Philadelphia: Soc. Ind. Applied Math, 1992.

[14] S. Mallat, "A theory for multiresolution signal decomposition: The wavelet representation," *IEEE Trans. Patt. Anal. Mach. Intell.*, vol. 11, no. 7, pp. 674–693, 1989.

[15] B. S. Manjunath and R. Chellappa, "A computational approach to boundary detection," *Proc. CVPR*, pp. 358–363, 1991.

[16] T. R. Reed and H. Wechsler, "Segmentation of textured images and gestalt organization using spatial/ spatial frequency representation," *IEEE Trans. Patt. Anal. Mach. Intell.*, vol. 12, pp. 1–12, Jan 1990.

[17] J. R. Bergen and M. S. Landy, "Computational modelling of visual texture segregation," in *Computational Models of Visual Processing* (M. S. Landy and J. A. Movshan, eds.), pp. 472–481, Cambridge, MA: The MIT Press, 1991.

[18] P. H. Carter, "Texture discrimination using wavelets," in *SPIE applications of digital image processing XIV*, vol. 1567, pp. 432–438, 1991.

[19] M. Unser and M. Eden, "Multiresolution feature extraction and selection for texture segmentation," *IEEE Trans. Patt. Anal. Mach. Intell.*, vol. 11, pp. 717–728, 1989.

[20] M. Unser, "Texture classification and segmentation using wavelet frames," *IEEE Transactions on Image Processing*, vol. 4, no. 11, pp. 1549–1560, 1995.

[21] T. Chang and C. C. J. Kuo, "Texture analysis and classification with tree structured wavelet transform," *IEEE Transactions on Image Processing*, vol. 2, no. 4, pp. 42–44, 1993.

[22] A. Laine and J. Fan, "Texture classification by wavelet packet signatures," *IEEE Trans. Patt. Anal. Mach. Intell.*, vol. 15, no. 11, pp. 1186–1190, 1993.

[23] F. S. Cohen, Z. Fan, and M. A. Patel, "Classification of rotation and scaled textured images using gaussian markov random field models," *IEEE Trans. Pattern Anal. Machine Intell. PAMI*, vol. 13, no. 2, pp. 192–202, 1991.

[24] J. L. Chen and A. Kundu, "Rotation and gray scale transform invariant texture identification using wavelet decomposition and hidden markov model," *IEEE Trans. Patt. Anal. Mach. Intell.*, vol. 16, no. 2, pp. 208–214, 1994.

[25] W. R. Wu and S. C. Wei, "Rotation and gray scale transform invariant texture classification using spiral resampling, subband decomposition and hidden markov model," *IEEE Trans. on Image Process.*, vol. 5, no. 10, pp. 1423–1434, 1996.

[26] S. R. Fountain and T. N. Tan, "Efficient rotation invariant texture features for content - based image retrieval," *Pattern Recognition*, vol. 31, no. 11, pp. 1725–1732, 1999.

[27] I. Daubechies, "Orthogonal bases for compactly supported wavelets," *Comm. Pure Appl. Math*, vol. 41, pp. 909–996. 1988.

[28] S. Mallat, "Zero-crossings of a wavelet transform," *IEEE Trans. Patt. Anal. Mach. Intell.*, vol. 37, no. 4, pp. 1019–1033. 1993.

[29] S. Mallat and S. Zhong, "Characterization of signals from multiscale edges," *IEEE Trans. Patt. Anal. Mach. Intell.*, vol. 14. no. 7, pp. 710–732. 1992.

[30] P. Brodazt, *Textures, A Photographic album for artists and designers.* New York: Dover Publications, 1966.

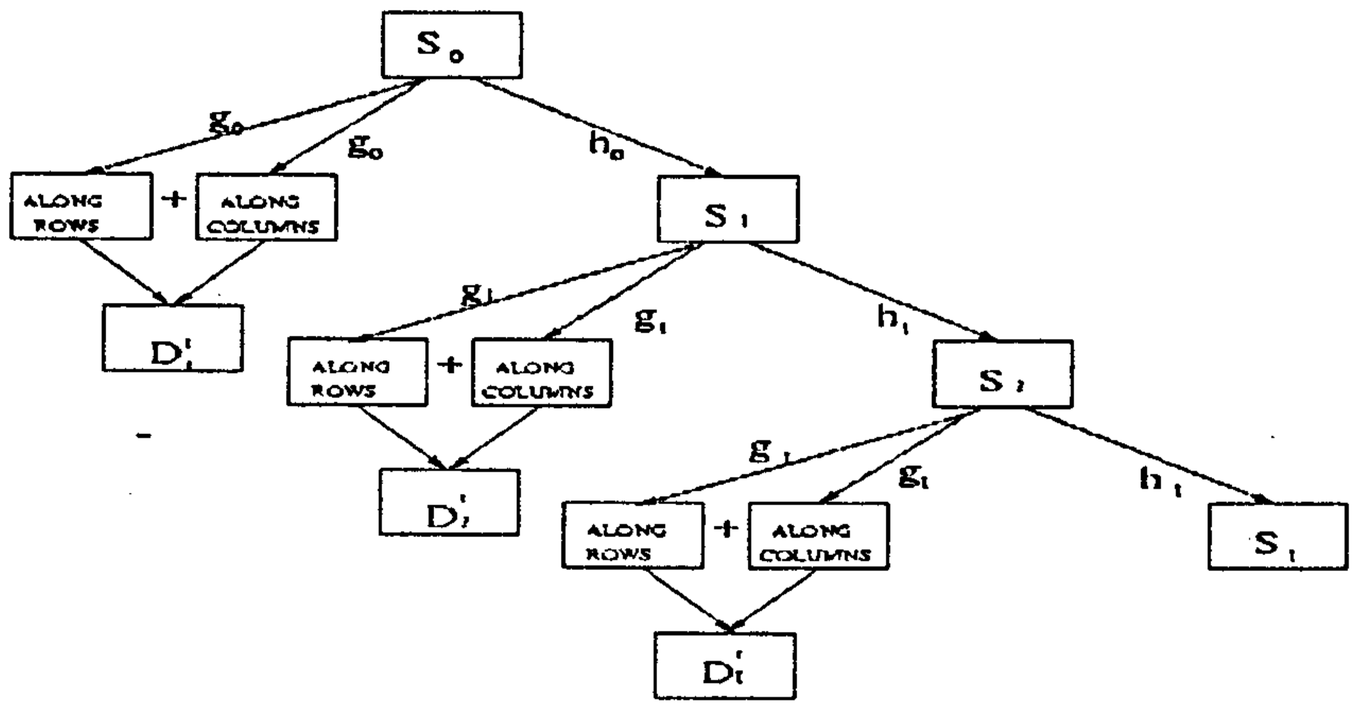

Figure 1: Fast iterative implementation of the algorithm used for extracting texture features

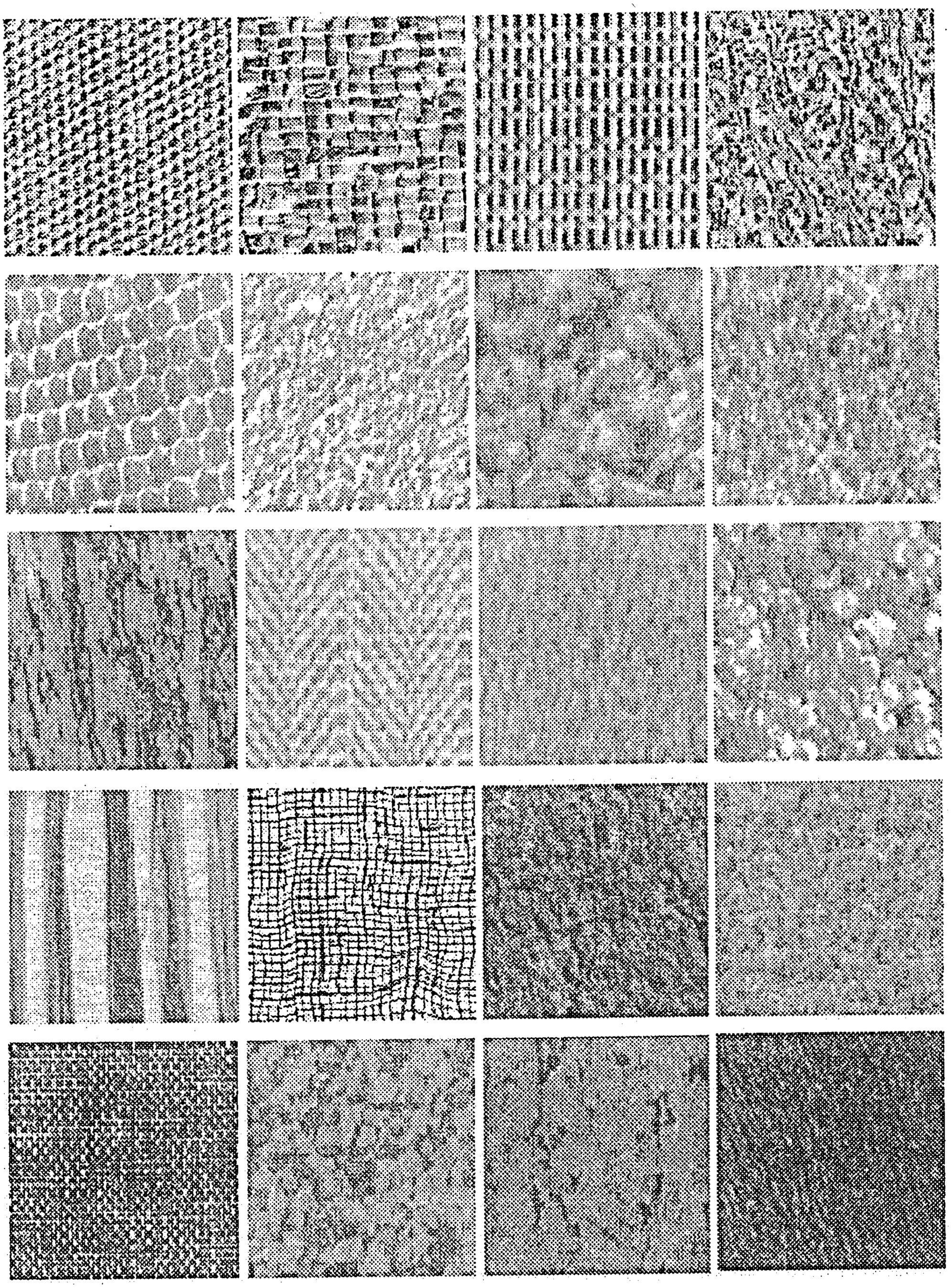

Figure 2: The textured images used in our experiment.

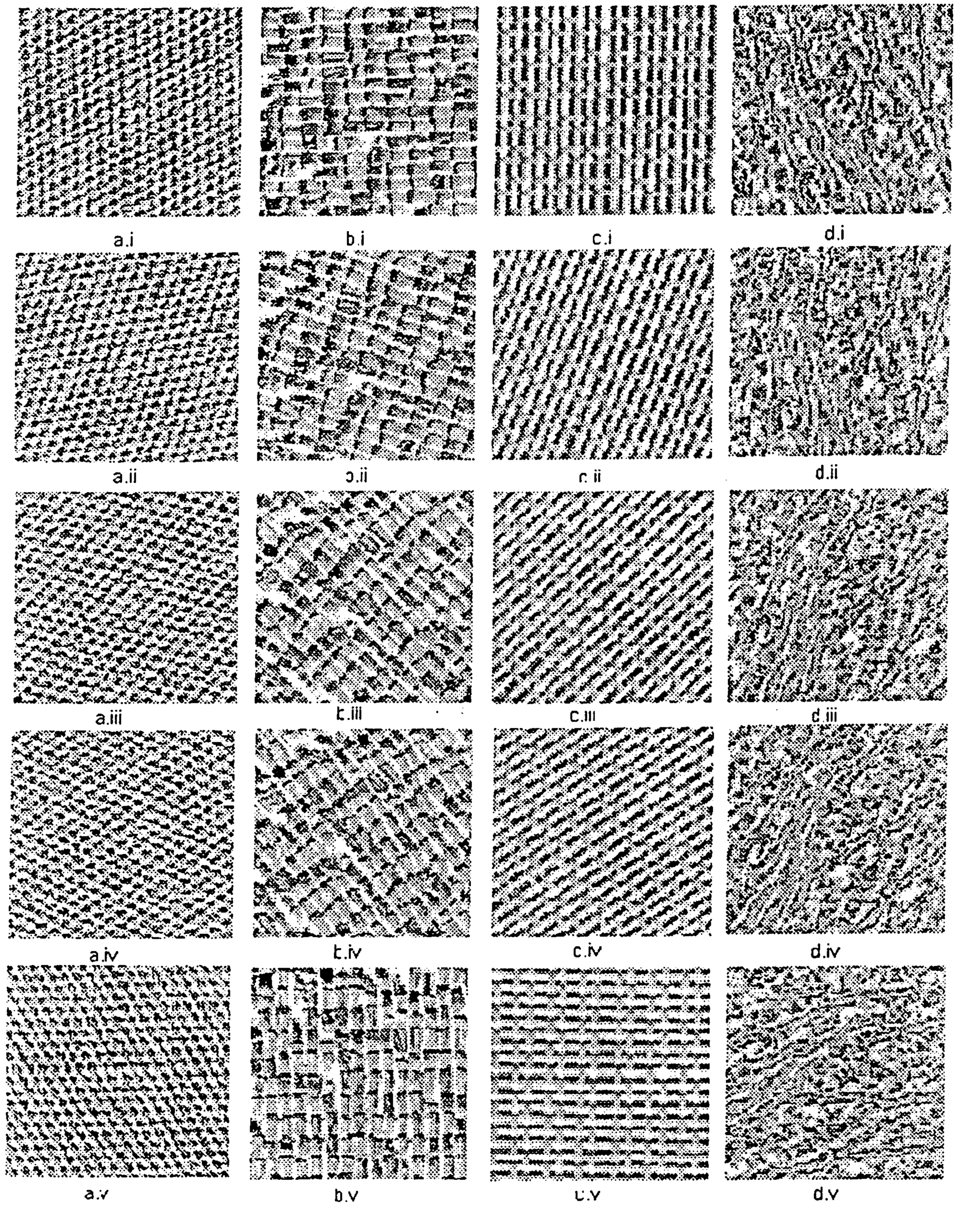

Figure 3: Rotated samples (0^0, 20^0, 45^0, 55^0, and 90^0) of some of the textured images used in our experiment.

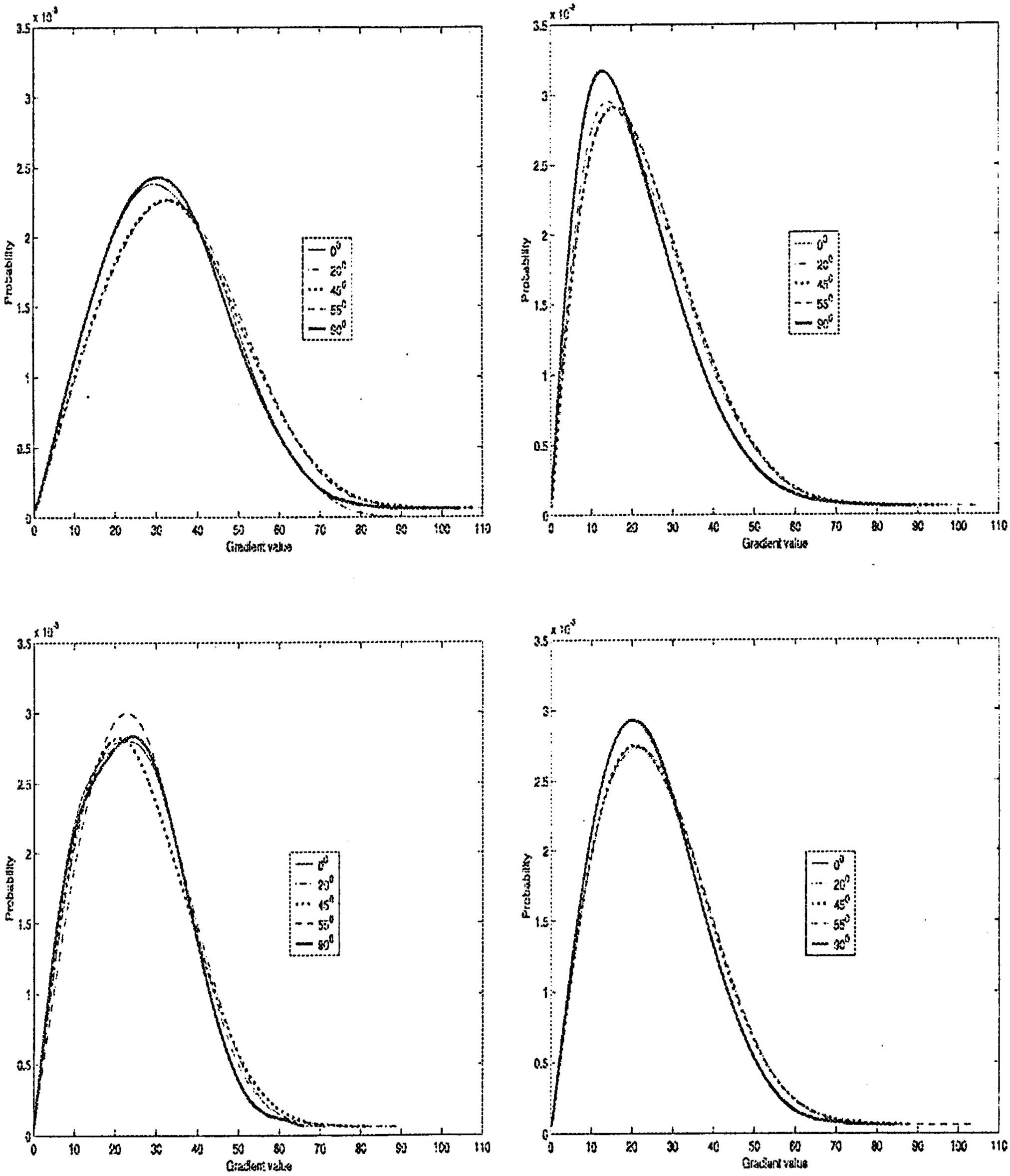

Figure 4: Edge magnitude histogram plots of textures shown in figure 3 for textures a)2.a.i - 2.a.v b)2.b.i - 2.b.v c)2.c.i - 2.c.v d)2.d.i - 2.d.v

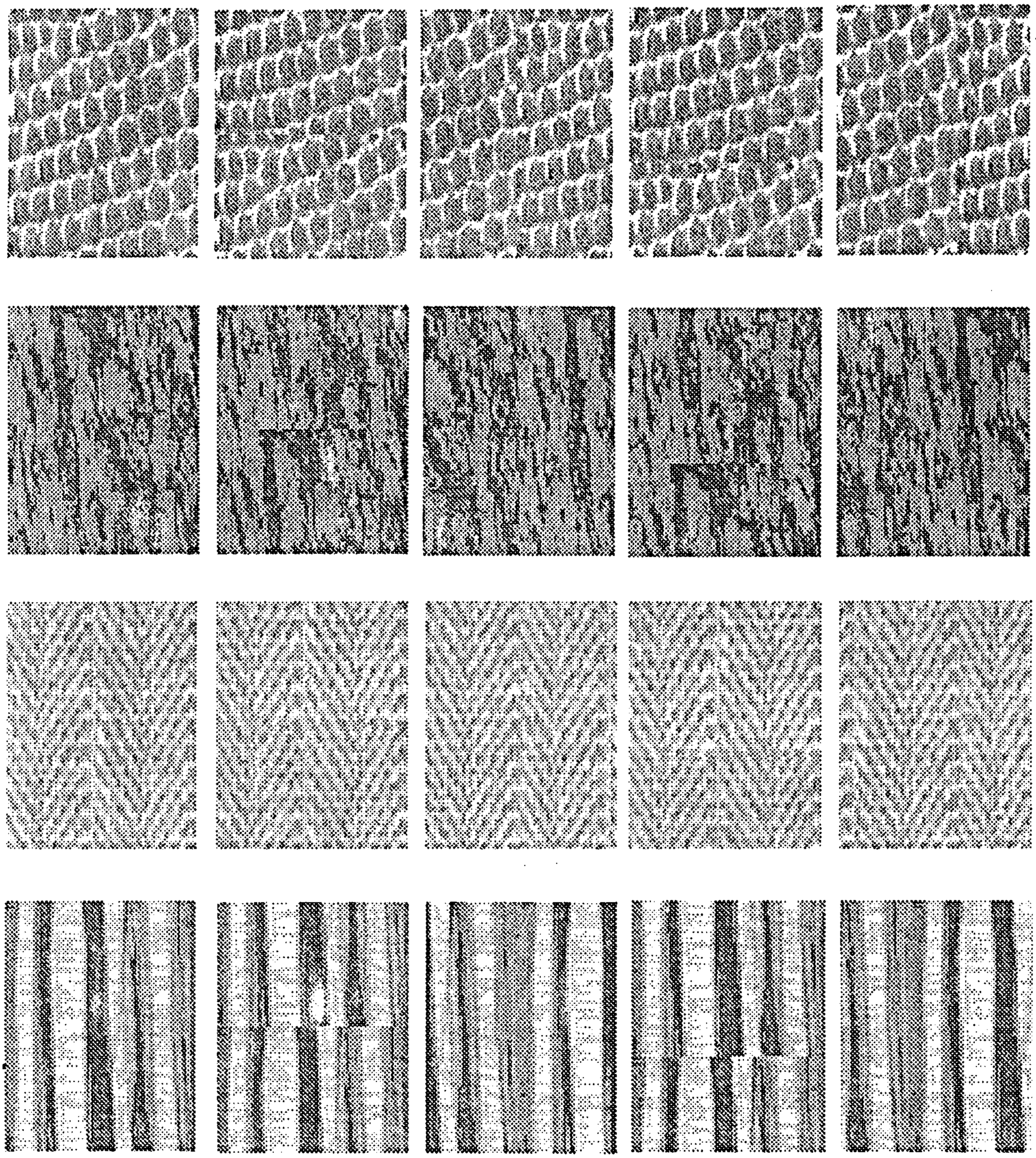

Figure 5: Translated samples of some of the textured images downshift - 64, 48 and rightshift - 64, 48.

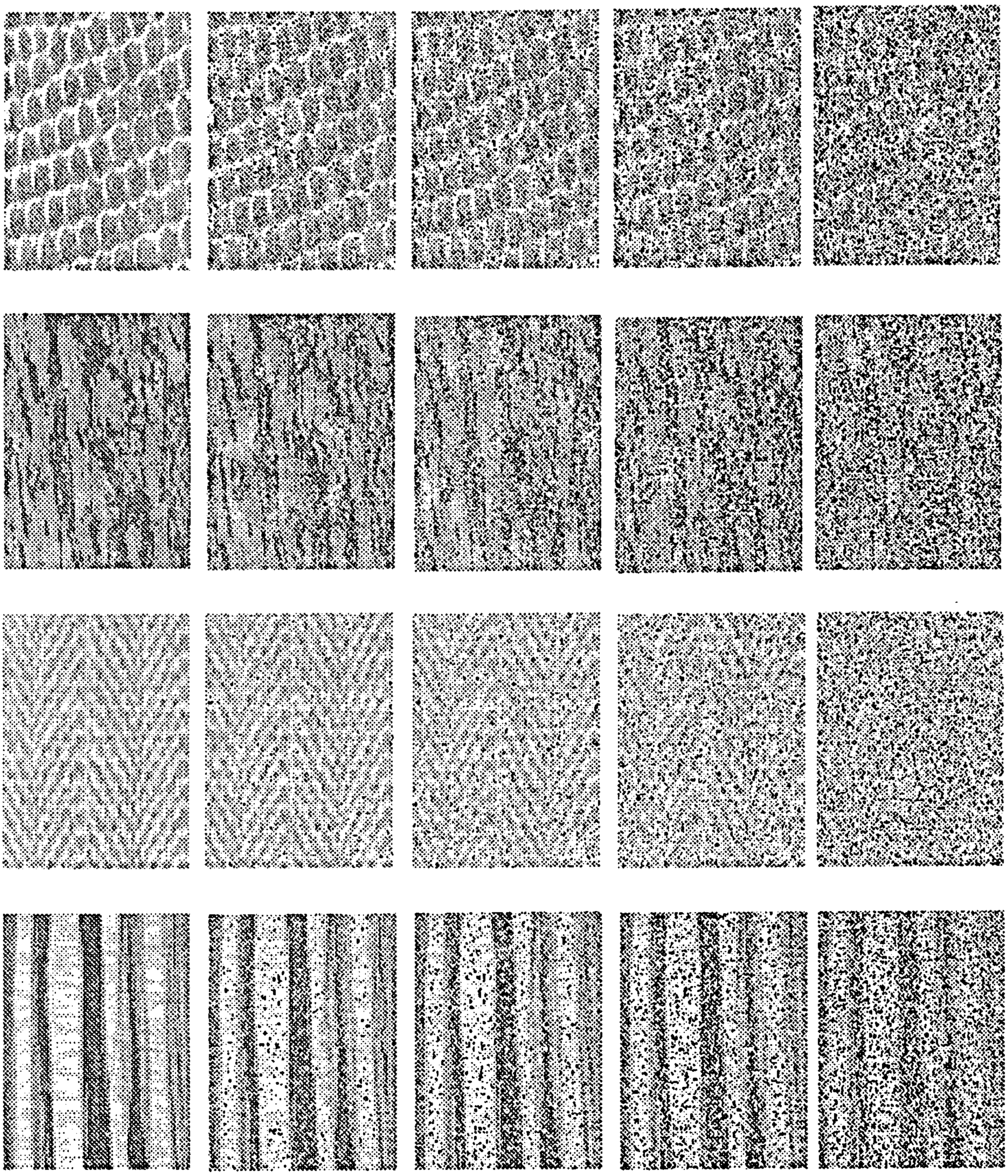

Figure 6: Noisy samples (15, 25, 30, 50 *db. noise level*) of some of the textured images used in our experiment.